Available online at www.sciencedirect.com
SCIENCE DIRECT
Journal of Catalysis 227 (2004) 408–418
JOURNAL OF CATALYSIS
www.elsevier.com/locate/jcat

$(NH_4)_2SiF_6$-modified ZSM-5 as catalysts for direct hydroxylation of benzene with N_2O 2. A comparative study with ferrisilicalite and dealuminated and iron-exchanged ZSM-5

Felix Kollmer, Heike Hausmann, Wolfgang F. Hoelderich *

Department of Chemical Technology, University of Technology RWTH Aachen, Worringerweg 1, 52074 Aachen, Germany

Received 10 February 2004; revised 24 June 2004; accepted 1 July 2004

Available online 15 September 2004

Abstract

The direct hydroxylation of benzene with nitrous oxide was studied over two HZSM-5 zeolites and over ferrisilicalite. HZSM-5 zeolite was dealuminated with $(NH_4)_2SiF_6$ as described previously, with steam treatment, with high-temperature calcination, and with steam treatment and subsequent acid wash. Furthermore one sample was exchanged with aqueous $Fe(NO_3)_3$, treated with $Na_2S_2O_4$, and acid-washed. The samples were characterized with regard to their elemental composition and textural, structural, and acid–base properties, using a variety of methods such ICP-AES, XRD, BET, NMR, FTIR, and ^1H and ^{27}Al MAS NMR. The catalytic performance was correlated to acid–base and textural properties of all the materials. Samples treated with $(NH_4)_2SiF_6$, according to a method developed in our laboratory, combined high activity with excellent resistance to deactivation compared to the other examined materials.

Keywords: Oxidation of benzene; Phenol; Dinitrogenoxide; Dealuminated ZSM-5; Lewis acidity

1. Introduction

Due to its industrial relevance, the direct synthesis of phenol starting from benzene and N_2O over modified pentasil zeolites has attracted the attention of numerous research groups in the past 15 years [1–14]. There is general agreement that the Na form and the Brønsted acid hydrogen of the material are moderately active, at best. Thus, several (post)synthetic treatment methods have been applied to optimize the performance of the catalyst. These treatments include the addition of iron, during hydrothermal synthesis [15], by aqueous exchange procedures [16,17] and CVD of $FeCl_3$ [18–20], high-temperature calcination, steam treatment [6,21], and treatment with $(NH_4)_2SiF_6$ [22].

Besides the question of activity and selectivity the rapid decline of catalytic activity due to the formation of carbonaceous deposits is at least one major obstacle to the commercial application of this promising catalyst system [23]. Only few studies (e.g., [24–28]) have addressed this problem and there is little reliable data concerning catalyst properties. In addition different ideas about the deactivation mechanism are discussed. Kustov et al. realized higher resistance to activity loss with higher pretreatment temperature [29] and assigned this effect to a lower density of bridging hydroxyl groups. Notté [10] reported a synergism of Brønsted acidity and α-siting upon phenol formation, but also a disadvantageous effect of Brønsted sites on the service time of the catalyst. McGhee and Notté [24] reported that the service time of the catalyst can be prolonged without affecting phenol productivity by removal of detrimental aluminum species by an acid wash after a steam treatment. This is somewhat contradictory to the findings of Motz et al. [6] who assume

* Corresponding author. Fax: +49 (0) 241 8022291.
E-mail address: hoelderich@rwth-aachen.de (W.F. Hoelderich).

0021-9517/$ – see front matter
doi:10.1016/j.jcat.2004.07.007

that extraframework aluminum species formed by mild hydrothermal treatment as active sites for benzene hydroxylation. McGhee [17] describes a favorable catalyst system in terms of activity and prolonged service time, which is obtained by postsynthetic introduction of iron and subsequent treatment with a reducing agent and a mineral acid. Ivanov et al. [26] found that the rate of phenol formation is correlated to the density α-sites on partially coked catalysts. Hence, it was concluded that catalyst deactivation proceeds by blocking the active site itself and that pore blocking by coke is not a decisive factor. Recently, we reported that the deactivation rate is related to the density of Brønsted acid sites and the rate of benzene hydroxylation is closely related to the density of Lewis acid sites and to the mesoporosity, which is created during dealumination of ZSM-5 by $(NH_4)_2SiF_6$.

A common problem in heterogeneous catalysis is the lack of comparability of materials prepared in different laboratories and the catalytic performance studied under different reaction conditions. To the best of our knowledge reliable data on the influence of several dealumination methods on the physicochemical properties and their catalytic performance in the benzene-to-phenol reaction have not yet been published. Hence, it was the aim of this comparative study to establish the above-noted correlations for a wider range of materials.

2. Experimental

2.1. Catalysts

The basis materials A-550 and B-550 were described elsewhere in detail [22]. Iron silicalite (FS) was obtained by hydrothermal synthesis (11 days, 190 °C, autogeneous pressure), starting from a gel consisting of 122.7 g SiO_2 (Ludox, HS40), 4.15 g $FeSO_4$, 9.16 g $NaHCO_3$, and 83 g aqueous TPAOH (20%). After filtration and washing with deionized water the solid was dried at 100 °C for 18 h and calcined in air at 450 °C for 48 h. The NH_4^+ form was obtained by eightfold ion exchange with an aqueous NH_3 solution (0.1 M). The solid was recovered by filtration and dried at 100 °C for 18 h. Subsequent calcination in air for 48 h at 450 °C yielded the proton form. The elemental composition of the basis materials is given in Table 1.

Hydrothermal treatment took place in a thermostated quartz tube at 550 and 650 °C at 500 mbar water partial pressure in N_2 for a given period of time. The sample names are A-*T*st-*t* for materials derived from the basis material A-550 and B-*T*st-*t* for materials derived from B-550. High-temperature calcination took place for 6 h in a thermostated quartz tube in a steady flow of dry N_2. The treatment temperatures were 800, 900, and 1000 °C and resulted in samples A-*T*T. *T* indicates the temperature of the treatment in both cases and *t* its duration in the case of steam treatment.

Sample A-650st-1ac0.5NO3 was obtained by acid treatment of A-650st-1 with 0.5 M HNO_3 at 70 °C for 3 h and subsequent calcination at 550 °C in air. Samples B-550st-6ac1NO3 and B-550st-6ac1Ox were derived from sample B-550st-6 after acid treatment with 1 M HNO_3 and $(COOH)_2$ at 70 °C for 3 h and subsequent calcination at 550 °C in air.

Table 1
Elemental composition of the basis materials, steamed- and acid-treated, and iron-modified samples

	Bulk chemical composition[a]		
	SiO_2/Al_2O_3	Na/Al	Fe[b] (wt%)
Basis material A			
A-550	30	< 0.02	0.02
A-650st-1	30	< 0.02	0.02
A-650st-1ac0.5NO3	31	< 0.02	0.02
A-st-1-Fe	30	< 0.02	0.17
A-st-1-Fe-S2O4	30	0.09	0.13
A-st-1-Fe-S2O4ac	32	< 0.02	0.12
Basis material B			
B-550	20	0.04	0.03
B-550st-6	20	0.04	0.03
B-550st-6ac1NO3	25	< 0.02	0.02
B-550st-6ac1Ox	24	< 0.02	0.015
Basis material FS			
FS-550st-14	$\sim 10^3$	~ 3	3

[a] Determined by ICP-AES.
[b] Based on Fe_2O_3.

Sample A-st-1-Fe was obtained by the threefold aqueous ion exchange of sample A-650st-1 with $Fe(NO_3)_3$ at 70 °C and subsequent calcination in air at 550 °C. Sample A-st-1-Fe-S2O4 was derived from sample A-st-1-Fe by the threefold treatment with an aqueous solution of $NaCl/Na_2S_2O_4$ (0.01 M) at 70 °C for 0.25 h and subsequent calcination in air at 550 °C. Sample A-st-1-Fe-S2O4ac was obtained from sample A-st-1-Fe-S_2O_4 by treatment with aqueous HNO_3/NH_4NO_3 (0.25 M) at 70 °C and subsequent air calcination at 550 °C.

The experimental details of dealumination with $(NH_4)_2SiF_6$ are given in detail elsewhere [22]. In brief, method (i) consisted of an aqueous procedure in a buffered solution and method (ii) was a solid-state procedure followed by thorough washing with large amounts of hot deionized water to give samples A-SiF6-100aq for method (i) and A-SiF6-100S-aq and for method (ii). Method (iii) consists of thermal decomposition of fluoro species left over from the preceding solid-state procedure leading to samples A-SiF6-*n*S and B-SiF6-*n*S. *n* denotes the degree of theoretical exchange, i.e., the molar ratio of SiF_6^{2-}/framework aluminum. Samples A-SiF6-100S and B-SiF6-100S were subjected to hydrothermal treatment at 550 °C as described above for 3 and 6 h, respectively, resulting in materials A-SiF6-100S-st3 and B-SiF6-100S-st6.

2.2. Characterization

The methods and equipment used for catalyst characterization were described in detail [22] elsewhere.

2.3. Catalytic tests

The experimental setup, the procedure, and the determination of activity and rate of deactivation are described [22]. Based on the definition given in [30] a Weisz number of $\sim 3 \times 10^{-3}$ was calculated based on space–time yields of 1 $g_{phenol}/(g_{cat}\,h)$ and an estimated macropore diameter within the catalyst pellet of 0.1 µm. Thus, a possible limitation of the reaction rate by external mass transport and pellet diffusion can be safely ruled out. With a crystallite diameter of 3 to 5 µm (vide infra) and an intracrystalline diffusivity of benzene in silicalite of $\sim 10^{-12}$–10^{-11} m^2/s (extrapolated from values in [31]) a Weisz number of 0.2–2 is obtained.

3. Results and discussion

3.1. Characterization

Elemental compositions of the basis materials, iron-modified, and steam- and acid-treated materials are given in Table 1. The aluminum content of both ZSM-5 samples is close to the upper limit. For this reason a zoning of framework aluminum (FAL) and, therefore, of acidity as observed by several research groups, e.g., [32], is unlikely. Intentional addition of Fe to the basis materials did not take place; the iron contents in basis material A-550 and B-550 are 0.02 and 0.03 wt%, respectively. These levels are in a range of the linear relation between catalytic activity and iron content observed by other research groups (e.g., [33]). Only trace amounts of aluminum were found on the iron silicalite sample (FS-550st-14) and the Si/Fe ratio is 40, i.e., the range in which Pirutko et al. [33] found the highest activity for borosilicalite and titanosilicalite with iron admixtures and Kharitanov et al. [15] for ferrisilicalite, respectively. Threefold aqueous ion exchange of the steamed basis material A-650st-1 increased the iron content by one order of magnitude compared to the parent material (A-st-1-Fe); however, complete exchange (Fe/Al = 0.33) was by far not reached due the large hydrate shell of Fe^{3+} in aqueous solution and the thermodynamic equilibrium, which favors the protic form of the zeolite [34]. The leaching procedure with $NaCl/NaS_2O_4$ leads to the selective removal of iron, in accordance with the reports of Derouane et al. [35] (A-st-1-Fe-S2O4), whereas a acid leaching with HNO_3 reduced both aluminum and iron (A-st-1-Fe-S2O4ac).

Mild acid treatment (A-650st-1ac0.5NO3) hardly changed the elemental composition, whereas treatment with 1 M HNO_3 and $(COOH)_2$ significantly reduced the amounts of aluminum and iron on sample B-550st-6. Despite the weaker strength compared to HNO_3, oxalic acid seems to be the more efficient agent, probably because it acts both as a proton donor and as a complexing agent.

The location and intensity of the infrared bands due to framework vibrations in the zeolites provide information about crystallinity, structure, and density of the heteroatoms ([36] and references therein). In ZSM-5 zeolites, a correlation between the framework aluminum content and the location of the band maximum of the asymmetric T–O vibration was established by Loeffler et al. [37]. Data on the shift of the IR band at 1100 cm^{-1} (Table 2) clearly indicate that framework dealumination takes place upon thermal and hydrothermal treatment.

The ^{27}Al MAS NMR (not shown) provided information concerning the coordination sphere of aluminum. The basis material before use showed a peak exclusively due to tetrahedrally coordinated aluminum, implying that all the NMR-visible aluminum is built into the zeolite framework or in an amorphous SiO_2/Al_2O_3 phase. A second peak at around 0 ppm is observed after catalytic testing, giving rise to the assumption that dealumination/dehydroxylation probably took place during regeneration at 550 °C. Dealumination under

Table 2
NMR and FTIR data of the (hydro)thermally treated materials

	NMR		PyFTIR				FTIR
	Al_{th}[a] (u.c.)	Al_{fr}[b] (u.c.)	$A_{Br,\,spec}$[c]	$A_{Le,\,spec}$[d]	A_{Le}/A_{Br}	$(A_{Br}+A_{Le})_{spec}$	$\Delta\nu$[e] (cm^{-1})
A-550	6.4	6.4	0.127	0.023	0.18	0.150	0
A-800T	4.3	2.5	0.058	0.035	0.60	0.089	2.7
A-900T	3.9	2.3	0.034	0.041	1.21	0.077	4.8
A-1000T	2.9	1.1	0.019	0.031	1.64	0.048	5.4
A-1080T	3.1	n.d.	0.008	0.008	1	0.016	5.7
A-650st-1	5.3	3.3	0.064	0.035	0.55	0.099	0.8
A-550st-3	3.8	2.0	0.048	0.029	0.60	0.077	4.8
A-550st-6	4.5	1.4	0.043	0.032	0.73	0.075	4.8
A-550st-14	4.5	0.9	0.030	0.022	0.73	0.052	4.8
B-550	8.3		0.176	0.033	0.18	0.209	0
B-550st-6	5.7		0.032	0.024	0.76	0.056	6.3

[a] From ^{27}Al MAS NMR.
[b] From ^{1}H MAS NMR.
[c] Band area of Brønsted-bonded pyridine at 150 °C related to the band area of the structural vibration.
[d] Band area of Lewis-bonded pyridine at 150 °C related to the band area of the structural vibration.
[e] Shift in the band maximum of the asymmetric T–O–T stretching vibration at $\sim$1100 cm^{-1}.

Table 3
NMR and FTIR data of hydrothermally and subsequently acid-treated materials

	NMR	PyFTIR				FTIR
	Al_{th}[a] (u.c.)	$A_{Br,\ spec}$[b]	$A_{Le,\ spec}$[c]	A_{Le}/A_{Br}	$(A_{Br}+A_{Le})_{spec}$	$\Delta\nu$[d] (cm^{-1})
A-550	6.4	0.127	0.023	0.18	0.150	0
A-650st-1	5.3	0.064	0.035	0.55	0.099	0.8
A-650st-1ac0.5NO3	5.6	0.068	0.035	0.51	0.103	1.2
B-550	8.3	0.176	0.033	0.18	0.209	0
B-550-st6	5.7	0.032	0.024	0.76	0.056	6.3
B-550-st6ac1NO3	4.6	0.049	0.019	0.40	0.068	7.1
B-550-st6ac1Ox	4.2	0.037	0.023	0.62	0.059	6.9

[a] From ^{27}Al NMR.
[b] Band area of Brønsted-bonded pyridine at 150 °C related to the band area of the structural vibration.
[c] Band area of Lewis-bonded pyridine at 150 °C related to the band area of the structural vibration.
[d] Shift in the band maximum of the asymmetric T–O–T stretching vibration at ∼ 1100 cm^{-1}.

relatively mild conditions has also been reported by other research groups. Müller et al. [38] lost 50% of FAL during the shallow-bed calcination of a HZSM-5 at 550 °C at ambient humidity and about the same percentage when the template of a NaBEA sample was removed under deep-bed conditions [39]. The intensity of the signal attributed to tetrahedral aluminum decreased when the material was exposed to more severe dealumination conditions. This effect has been studied quantitatively (Table 2). Moreover the signal at 0–2 ppm gains intensity and a new signal with a chemical shift of 30–33 ppm is observed, generally assigned to penta-coordinated [40–43] or distorted tetrahedral [44–46] aluminum species.

Interestingly, the ^{27}Al NMR spectra of tempered and steamed samples seem to be qualitatively more or less the same (Table 3). Even though it is well known that aluminum can be invisible to NMR, when present in a highly distorted coordination sphere (e.g., [39]), this fact does not support the idea of the formation of distinctly different kinds of Lewis acidity (LA), explicitally trigonally FAL, when pretreated under dry conditions, and octahedrally coordinated extraframework aluminum (EFAL), when pretreatment occurrs in a water-containing atmosphere as proposed by Kazansky [47] based on a DRIFT study of chemisorbed hydrogen. Also modification of ^{27}Al NMR spectra upon acid treatment can hardly be observed, indicating that a selective removal of EFAL does not take place.

FTIR spectra of the dehydrated thermally treated and hydrothermally treated materials are shown in Figs. 1 and 2, respectively. Bands at 3740, 3670–3640, and 3610 cm^{-1} are seen observed on all the materials. For both methods, steaming and calcining, the band of bridged hydroxyls at 3610 cm^{-1} decreases with increasing severity of the treatment due to dehydroxylation/framework dealumination and/or the formation of cationic EFAL, which replaces protons as charge compensation. However, the high-temperature treatment under the applied conditions seems to be the more efficient way to reduce the density of the BA sites. This is supported by the band area of chemisorbed pyridine on the BA sites (Table 2).

In the case of exposure to steam at 550 °C, a band at 3780 cm^{-1} appears and vanishes upon interaction with pyridine (not shown); this band is not observed on calcining or on steaming at 650 °C. Some authors attribute this band to transient aluminum species [48,49], others to hydroxyl groups on EFAL [50]; all authors reported an interaction

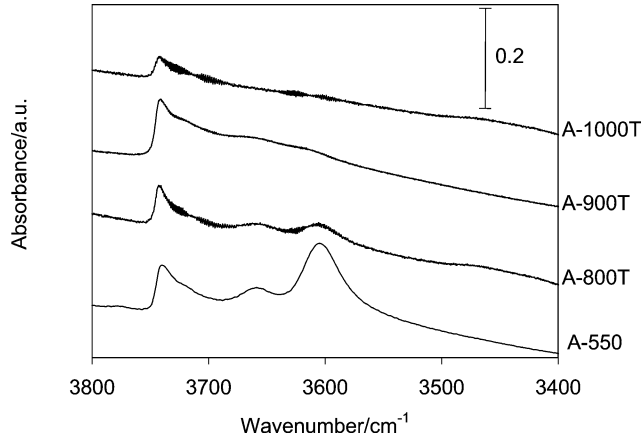

Fig. 1. FTIR spectra of the hydroxyl region of the basis material (A-550) and the calcined samples (A-800T, A-900T, A-1000T). Samples derived from basis material A-550.

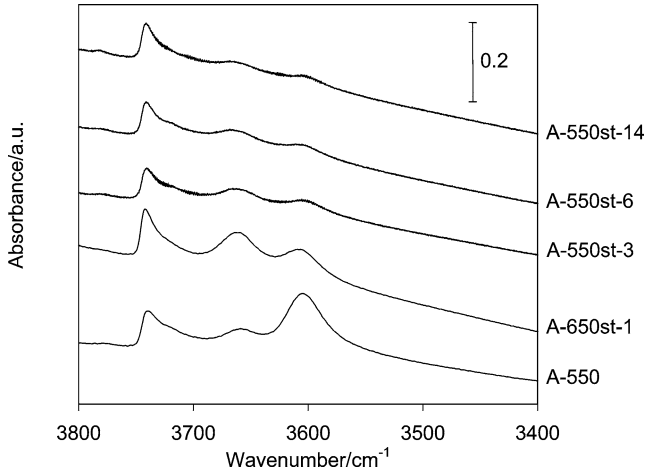

Fig. 2. FTIR spectra of the hydroxyl region of the basis material (A-550) and the hydrothermally treated samples (A-650st-1, A-550st-3, A-550st-6, A-550st-14). Samples derived from basis material A-550.

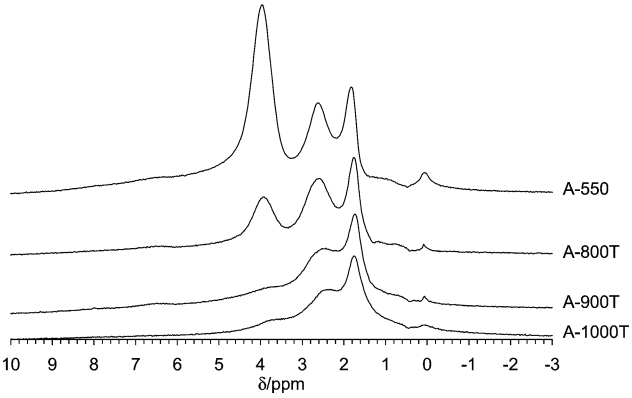

Fig. 3. ^{1}H MAS NMR spectra of the basis material (A-550) and calcined samples (A-800T, A-900T, A-1000T). Samples derived from basis material A-550.

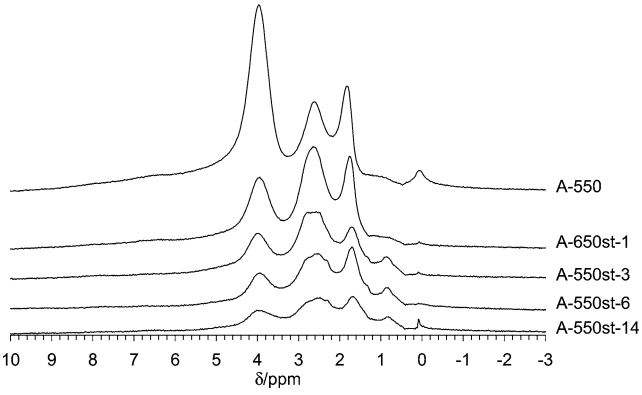

Fig. 4. ^{1}H MAS NMR spectra of the basis material A-550 and hydrothermally treated samples (A-650st-1, A-550st-3, A-550st-6, A-550st-14). Samples derived from basis material A-550.

with basic probe molecules. Loeffler et al. [50] reported thermostability of this band up to 750 °C. The fact that it is not observed on A-800T may indicate that another mechanism of dealumination is effective at higher temperatures. The band at 3665 cm^{-1} is not clearly assigned either. Some authors propose OH groups on EFAL [37,48], others OH on transient aluminum [50,51]. All authors have reported slight acidity, which has also been observed in the present work. The band gains intensity during steaming but it decreases after prolonged treatment and at higher temperatures, in line with both possibilities. However the band is also present in the basis material which can be either due to uncrystallized material from synthesis or to crystalline changes during sample preparation (template removal, calcination procedures, evacuation prior to FTIR measurement). Partial dehydroxylation would also explain the comparably high fraction of LA already in the basis material (Table 2).

These findings for the hydroxyl groups are supported by ^{1}H MAS NMR spectra (Figs. 3 and 4). There is an appreciable amount of OH groups bonded to EFAL ($\delta_h \sim 2.6$ ppm) already present in the basis material, which had been dehydrated in a similar manner for the NMR and FTIR measurements. The signal at 2.6 ppm follows the same trend as the infrared band at 3665 cm^{-1}. Samples steamed at 550 °C show the VHF band in the infrared spectrum (3780 cm^{-1}) and are also the only samples which show a weak NMR band at a chemical shift of ~ 0.8 ppm, giving rise to the assumption that the same species is responsible for those signals. Signals with a chemical shift of 0–0.7 ppm were previously assigned to unperturbed Al–OH, i.e., Al–OH which does not interact by hydrogen bonds [52,53].

For the signals of the bridged Si(OH)Al groups there is also a parallel trend in ^{1}H NMR ($\delta_h \sim 3.9$ ppm) and FTIR ($\nu \sim 3610$ cm^{-1}). However, the amount of tetrahedrally coordinated aluminum, calculated from ^{27}Al NMR, always exceeds in all cases the amount of BA protons, indicating that not all the species giving rise to the signal at $\delta_{Al} \sim 55$ ppm bear a proton but may instead bear cationic EFAL as charge compensation (Table 2).

Both high temperature and steam treatment lead to a shift in the acidity spectrum from Brønsted to Lewis acidity. Whereas the density of bridged hydroxyl groups decreases monotonously with increasing severity of the treatment, the density of the Lewis acid sites goes through a maximum during calcination and during steam treatment. Such a decrease under more severe treatment conditions can be attributed to the oligomerization and polymerization of EFAL and has also been observed by other groups [6,54–58]. This is consistent with the fact that the sum of the specific band areas decreases with increasing severity of the treatment (Table 2), if one is assuming a constant ratio of $\varepsilon_{Le}/\varepsilon_{Br}$ for the absorbance coefficients of pyridine on LA and BA sites of 1.2–1.5 [59–63]. In other words, the deeper the dealumination, the lower the ratio of aluminum contributing to any kind of acidity, regardless of whether steam or high-temperature treatment is applied. Roughly the same stoichiometry for the formation of LA from BA sites is found for both methods (Table 2). However, to create a high density of LA sites high-temperature calcination seems to be more efficient than steam treatment (Table 2). This is explained by the higher mobility of extraframework species under hydrothermal conditions, leading to a higher rate of polymerization of EFAL. For subsequently acid-treated samples, a slight increase in the density of Brønsted sites (Table 3) is attributed to the ion exchange of cationic EFAL species with protons. But the shift of the T–O vibration indicates further framework dealumination. The limited solubility of Lewis acid extraframework species is in agreement with previous reports by Brunner et al. [64].

Temperature-programmed desorption of pyridine (PyTPD) yields information about the strength of the acid sites (Fig. 5). A significant difference between calcined and steamed material is not found, indicating that the materials are indeed very similar with respect to their acid–base properties. In the case of Brønsted acidity, ^{1}H NMR confirms this finding as the shift of the signal for bridged Si(OH)Al does not indicate a change in acid strength upon dealumination with either method. However, on both materials adsorption of pyridine on Brønsted sites is significantly weaker than on Lewis sites. This may explain the high-temperature peak fre-

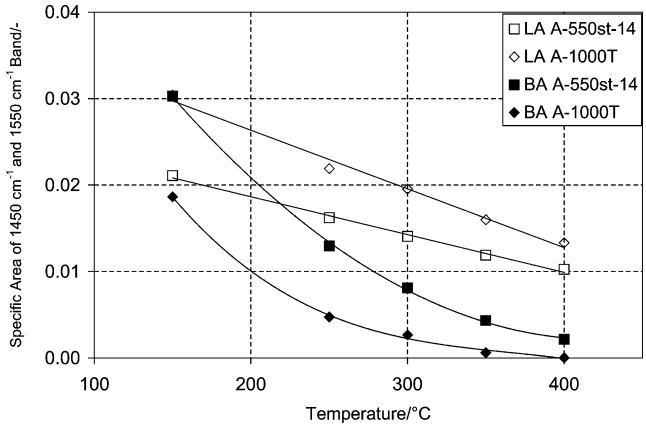

Fig. 5. Specific band areas of Brønsted- and Lewis-adsorbed pyridine as a function of temperature (samples A-1000T and A-550st-14).

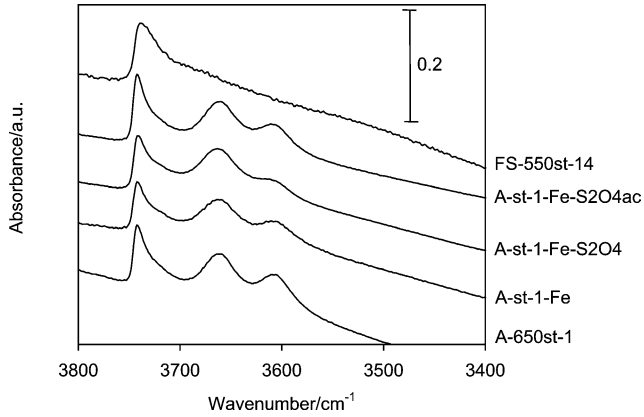

Fig. 6. FTIR spectra of the hydroxyl region of hydrothermally treated ferrisilicalite (FS-550st-14) and hydrothermally and hydrothermally + iron-modified samples (A-650st-1, A-st-1-Fe, A-st-1-Fe-S2O4, A-st-1-Fe-S2O4ac).

quently reported in NH_3 TPD of dealuminated materials and attributed to the superacidity in zeolites [65,66].

Infrared spectra of the hydroxyl region of steamed iron silicalite is depicted in Fig. 6. Hydrothermal treatment of ferrisilicalite results in deep demetallation, as seen from the complete absence of the band at 3650 cm^{-1}, characteristic of bridging Si(OH)Fe groups [67], and from the low level of Brønsted-bonded pyridine (Table 4). The lower hydrothermal stability of iron silicalite compared to HZSM-5 has also been reported by other researchers [68] and is attributed to the greater ionic radius of Fe^{3+} compared to Al^{3+} [69]. The density of the defect sites due to extraction of iron out of the zeolite lattice is higher compared to aluminum-containing materials as seen by the shoulder at 3720–3730 cm^{-1} and the broad peak at $\sim$ 3500 cm^{-1}. However, Lewis acidity (Table 4) is also much lower compared to the steamed ZSM-5, indicating a high mobility of the extraframework iron species under hydrothermal conditions. Despite the effective removal of framework iron, the integrity of the silica backbone is preserved, as seen from the XRD diffractions (not shown) and the high microporous volume determined by physisorption of N_2 ($V_{micro} = 0.14\ ml\ g^{-1}$).

FTIR spectra of the hydroxyl region (Fig. 6) and pyridine adsorption data (Table 4) show a slight decrease in the level of the BA sites after Fe loading, in accordance with the ion exchange of Brønsted protons. The subsequent treatment with $S_2O_4^{2-}$ led to partial exchange of sodium ions up to 9% (Table 1). As a consequence the infrared band at 3610 cm^{-1}, due to bridging hydroxyls, and the specific band for Brønsted-bonded pyridine (Table 1) lose intensity. Both bands are restored after removal of Na^+ upon acid treatment (A-st-1-Fe-S2O4ac). Neither the hydroxyl groups on EFAL nor the level of the Lewis acid sites are affected substantially by the different treatments, as can be seen from the band at 3665 cm^{-1} in the infrared spectra (Fig. 6) and the specific band area of the Lewis-bonded pyridine (Table 4). ^{27}Al NMR spectra (not shown) support these observations, since the state of the Al nuclei hardly changes upon the post-synthetic introduction of Fe and subsequent treatments. The signals lose intensity upon iron loading and are successively restored after the subsequent leaching procedures (Table 4). This is due to the paramagnetism of the Fe nuclei and has been reported by other authors [70].

The impacts of the different dealumination and modification methods on the pore structure can be assessed based on the N_2 physisorption data in Fig. 7. With conventional methods, i.e., high temperature, steam, steam and acid treatments, and $(NH_4)_2SiF_6$ in aqueous solution and solid state, a considerable downgrade of Brønsted acid ($\sim$ 80%) sites is easily achieved without significant loss in microporosity, i.e., crystallinity. However, a further decrease in Brønsted acidity with conventional methods, such as high-temperature calcination at 1080 °C (A-1080T), leads to a substantial loss

Table 4
NMR and FTIR data of iron-containing materials

	NMR	PyFTIR			
	Al_{th}[a] (u.c.)	$A_{Br,\ spec}$[b]	$A_{Le,\ spec}$[c]	A_{Le}/A_{Br}	$(A_{Br} + A_{Le})_{spec}$
FS-550st-14	–	0.002	0.005	2.121	0.007
A-650st-1[c]	5.3	0.064	0.035	0.55	0.099
A-st-1-Fe	3.9	0.057	0.028	0.49	0.084
A-st-1-Fe-S2O4	4.1	0.056	0.029	0.51	0.086
A-st-1-Fe-S2O4ac	4.6	0.067	0.031	0.45	0.098

[a] Determined by ^{27}Al NMR.
[b] Band area of Brønsted-bonded pyridine at 150 °C related to the band area of the structural vibration.
[c] Band area of Lewis-bonded pyridine at 150 °C related to the band area of the structural vibration.

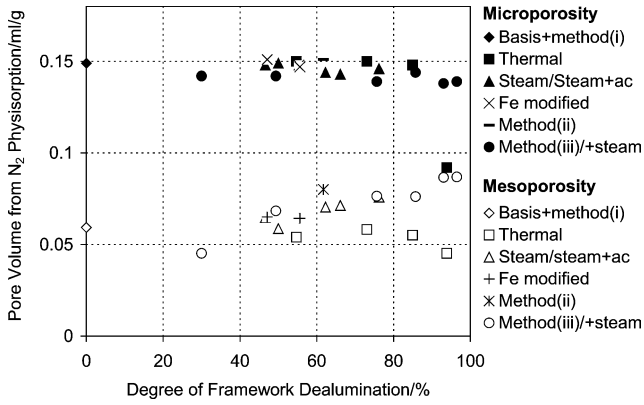

Fig. 7. Specific pore volumes of basis material (A-550), calcined (A-800T, A-900T, A-1000T, A-1080T), steamed (A-650st-1, A-550st-3, A-550st-6, A-550-st-14), steamed + acid treated (A-650st-1ac0.5NO3), $(NH_4)_2SiF_6$ dealuminated (A-SiF6-100aq, A-SiF6-100S-aq, A-SiF6-20S, A-SiF6-40S, A-SiF6-60S, A-SiF6-100S, A-SiF6-100S-st3), and iron-modified materials (A-st-1-Fe, A-st-1-Fe-S2O4, A-st-1-Fe-S2O4ac) as a function of the degree of dealumination. Samples derived from basis material A-550.

of crystallinity and, thus, to a decrease of the catalytically active volume of the zeolite. Treatment with $(NH_4)_2SiF_6$ with method (iii), however, enables the deepest dealumination of all the methods while preserving the structural integrity.

In contrast to high-temperature calcination and aqueous treatment with $(NH_4)_2SiF_6$ (method (i)), steaming, steaming followed by acid leaching, and dealumination with $(NH_4)_2SiF_6$ according to methods (ii) and (iii) result in an increase in the mesoporous volume, generally associated with the formation of a secondary pore structure. This effect is frequently reported as consequence of steam and steam/acid treatment and is explained by a certain mobility of the silicon species from the amorphous material or heavily damaged zones that can refill framework defects formed upon removal of framework aluminum (see, e.g., [34] and references therein). A similar mechanism is for materials modified according to method (iii), since it is assumed that thermal decomposition of hexafluoro complexes after solid-state substitution leads to volatile, very mobile silicon species, such as SiF_4. This has been recently supported by the characterization of such materials [22]. This effect in combination with the deepest dealumination leads to materials with the highest mesoporosity of all the methods under consideration. For calcined materials the texture hardly changes up to treatment temperatures of 1000 °C, implying that mobility of extraframework species is rather limited under dry conditions. This is in line with the high concentration of Lewis acid sites on calcined compared to steamed samples (Table 2), indicating a higher dispersion and thus a slower oligomerization and polymerization of the EFAL species.

3.2. Catalysis

Figs. 8–10 give the rate constant of deactivation k_d and the density of the Brønsted acid sites at different reaction temperatures. In all cases, a clear correlation is found over

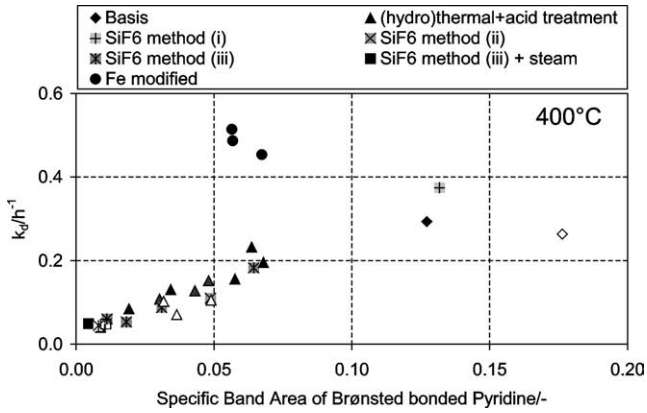

Fig. 8. Deactivation rate constant k_d as function of Brønsted acidity. $W/F = 20$ kg_{cat} s/mol, $C_6H_6/N_2O/N_2 = 4/2/1$ (molar), $S > 95\%$, 400 °C. Parameter is the modification method (filled symbols, samples derived from basis material A-550; open symbols, samples derived from basis material B-550).

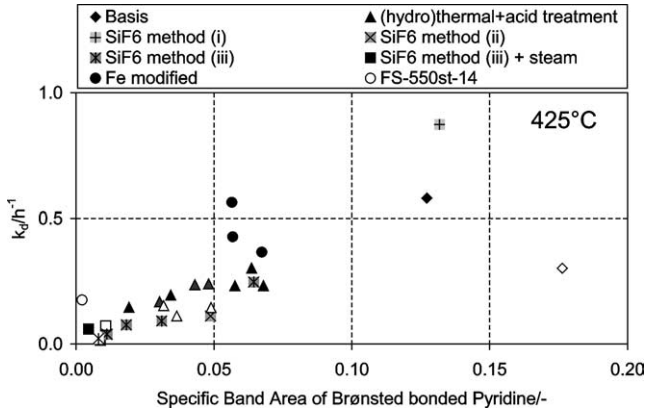

Fig. 9. Deactivation rate constant k_d as function of Brønsted acidity. $W/F = 20$ kg_{cat} s/mol, $C_6H_6/N_2O/N_2 = 4/2/1$ (molar), $S > 95\%$, 425 °C. Parameter is the modification method (filled symbols, samples derived from basis material A-550; open symbols, samples derived from basis material B-550).

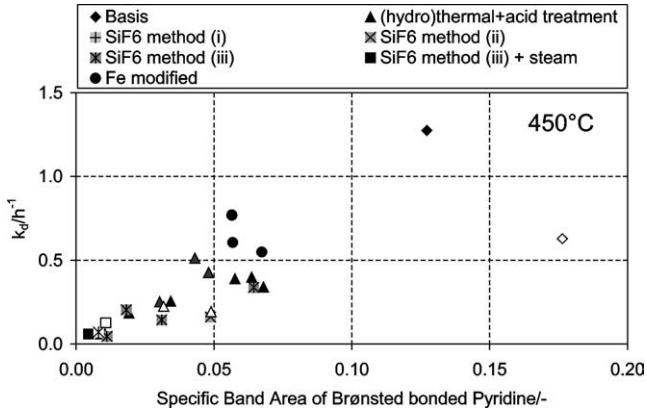

Fig. 10. Deactivation rate constant k_d as function of Brønsted acidity. $W/F = 20$ kg_{cat} s/mol, $C_6H_6/N_2O/N_2 = 4/2/1$ (molar), $S > 95\%$, 450 °C. Parameter is the modification method (filled symbols, samples derived from basis material A-550; open symbols, samples derived from basis material B-550).

dealuminated ZSM-5 derived from two different basis materials regardless of the method. For a comparable level of Brønsted acidity, deactivation occurs faster on materials with the intentional addition of iron no matter whether the iron was introduced during hydrothermal synthesis (FS-550st-14) or by means of postsynthesis methods (A-st-1-Fe, A-st-1-Fe-S2O4, A-st-1-Fe-S2O4ac). This is somewhat surprising, because it is generally agreed that Brønsted acidity originating from tetrahedrally coordinated iron, e.g., in ferrisilicalite, is supposed to be weaker than originating from framework aluminum in zeolitic systems (e.g., [69] and references therein).

These results strongly imply that the level of Brønsted acidity is the key factor in catalyst deactivation. However, based on the results obtained by now, we cannot yet conclude whether it is the only determining factor. The trends depicted in Figs. 8–10 show some scattering of the values, which increase with increasing reaction temperature. It is seen, however, that materials modified with SiF_6^{2-} in a solid-state procedure (method (ii) + (iii)) always perform better than conventional materials.

Moreover, due to the dispersion of the experimental values it is difficult to say, whether the trend can be extrapolated exactly to the origin, i.e., that in the case of the absence of Brønsted acidity, the catalyst remains active on a constant level throughout the reaction time. For a reaction temperature of 400 °C the trend seems to have an intercept for zero Brønsted acidity (Fig. 8), whereas at elevated temperatures (425 and 450 °C) this intercept is substantially smaller if not even zero (Figs. 9 and 10). If the intercept has a value unequal to zero, this would imply, that there is a second deactivation mechanism, possibly caused by strong adsorption of phenol on the active site. This desorption limitation can then be overcome by increasing the reaction temperature, in agreement with the results in the figures above. Such findings were reported previously by Burch and Howitt [25], who distinguished between "soft" coke, removable by treatment with N_2 at 500 °C, and "hard" coke on BA sites, only removable by oxidation.

Fig. 11 shows the initial conversion of benzene as a function of the density of the Lewis acid sites. Since it was observed that mesoporosity, created during dealumination [22], and crystallite size [71] might play a decisive role in the direct hydroxylation of aromatics, the materials have been grouped according to the mesoporous volumes derived by N_2 physisorption. There are reasonable correlations between Lewis acidity and the activity of the dealuminated materials, derived from both basis materials A and B, regardless of the treatment.

Hydrothermally treated ferrisilicalite also fits this pattern (Fig. 11), whereas postsynthetically modified ZSM-5 displays a higher initial activity as expected from its level of Lewis acidity and its mesoporous volume. This peculiarity will be discussed in detail below.

It is commonly experienced in heterogeneous catalysis that mass and heat transport affect the overall rate of the

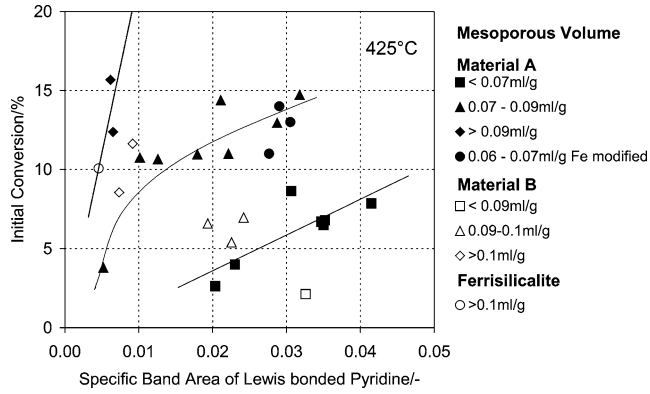

Fig. 11. Initial conversion of benzene as a function of Lewis acidity. Parameter: mesoporous volume. $W/F = 20$ kg_{cat} s/mol, $C_6H_6/N_2O/N_2 \approx 4/2/1$ (molar), $S > 95\%$, 425 °C (filled symbols, samples derived from basis material A-550; open symbols, samples derived from basis material B-550).

chemical conversion. This applies above all to fast chemical reactions, such as oxidations, which take place over a porous catalyst. If the characteristic time constant of diffusion ($\tau_{diff} = L^2/D$) is much higher than the characteristic time constant of the chemical reaction ($\tau_r = k_{r,i}^{-1}$), concentration gradients of the reactants arise within the catalyst particle and also between the particle surface and the surrounding gas phase; i.e., mass transport is the rate-limiting step of the overall procedure (e.g., [72]). This can lead to decreasing selectivity of reaction intermediates due to extended residence time on the catalyst and to lower conversion due to restricted accessibility of the active site.

The dimensionless group *We*, proposed by Weisz [73], should be < 0.3–1 in order to ensure an effectiveness factor of $\eta = k_{r,app}/k_{r,i} \geqslant 95\%$. However, it has been estimated to values of ~ 0.2–2 based on data of the catalytic materials determined in the present work and micropore diffusion of benzene. This value is in the vicinity to the one estimated by Louis et al. [8]. Bearing in mind the large discrepancies of diffusivities of hydrocarbons in zeolites reported in the literature (see, e.g., [31] and references therein), usually under conditions much different than those of the chemical reactions anyway, it is reasonable to assume that the reaction takes place in a transition regime, in which only active sites located in the outer shell of the zeolite crystallite take part. Thus, an increase in mesoporous volume upon dealumination, related to the formation of a secondary pore system, provides better access to the active site by shortening the characteristic length of diffusion L_{diff}. Therefore for a comparable level of Lewis acidity, materials with higher mesoporosity show higher initial activity. A synergetic effect of Brønsted acidity on activity, as postulated by Notté [10], is not supported by the results of the present work. On the contrary, materials with the lowest levels of BA, such as those treated with $(NH_4)_2SiF_6$ according to method (iii) and subsequently steamed, are among the most active catalysts. Notté based his assumption on a study of steamed ZSM-5 catalysts, which were subsequently ion exchanged

with Na. The most effective ion exchange was achieved by applying a basic buffer solution. Catalytic activity and the density of the α-sites, determined by stoichiometric N_2O decomposition, decreased with increasing ion-exchange degree, whereas the equilibrium sorption capacity for benzene remained constant. Hence, it was assumed that the removal of BA was selective; i.e., neither Lewis acidity nor the transport properties were affected by ion exchange. But this might be too simple an explanation. Experimental evidence is necessary, since extraframework aluminum and iron species can be in charge-compensating positions and can be removed by aqueous ion exchange. If this procedure occurrs in a slightly basic medium, reinsertion of EFAL [74] and reversibility of dehydroxylation are also reported [75], thus decreasing the density of the Lewis acid sites.

Furthermore, since the kinetic diameter of an aromatic ring is in close vicinity of the channel diameter of MFI, it is expected that the mobility of the reactants in the micropores is greatly affected by introducing bulky cations such as Na^+ with an ionic radius of 1.02×10^{-10} m [76]. Sorption properties are also significantly enhanced by the introduction of Na^+, resulting in Henry constants for benzene and phenol of one order of magnitude higher than in the protic form, as demonstrated by Klemm et al. [77]. It has been observed that the type of cation [78] and the presence of chemisorbed molecules [31,79] can have a significant impact on intracrystalline diffusivities. Moreover, in order to explain the essential role of BA, it was argued that addition of trace amounts of NH_3 to the feed also had a strong, but reversible impact on phenol productivity. But it has been shown previously [80] and in the present work that chemisorption of N bases such as pyridine is even stronger on Lewis sites than on Brønsted sites (Fig. 5). Hence, from this observation it can only be concluded that the reaction mechanism is not exclusively a redox type, but also involves acid–base interactions, whatever their nature.

Semilogarithmic plots of conversion as a function of time on stream of iron-containing materials are shown in Fig. 12. In contrast to dealuminated HZSM-5 (e.g., A-650st-1), materials with intentional introduction of Fe do not obey a first order deactivation rate–time law as seen from the concave shape of the curves. Together with the fact that activity and deactivation rate of iron-modified materials can hardly be correlated with the acid properties and textural properties (see above), this observation may indicate that on these materials the reaction is catalyzed by different active sites at different rates of the elementary steps, maybe even with a different reaction mechanism. It should be noted that for reasons of comparability curves of the iron-modified samples were evaluated by linear regression. Due to the concave shape, i.e., quicker activity loss at higher activity than for ordinary materials with linear shaped curves, the introduction of Fe leads to poorer materials.

Under identical reaction conditions, postsynthetically modified materials suffer quicker activity loss than the steamed staring material A-650st-1. Such a rapid decrease in the activity of iron-containing material compared to steamed ZSM-5 has also been observed by Zhu et al. [20].

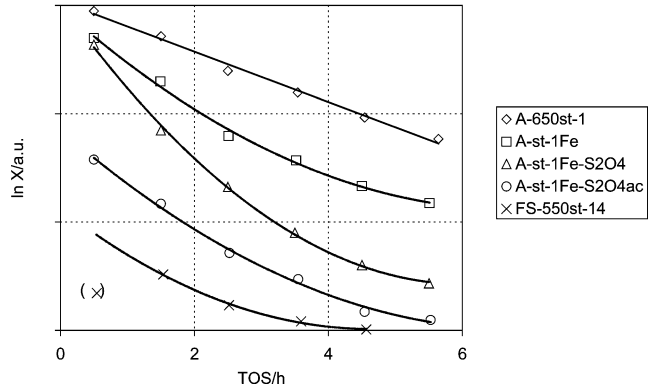

Fig. 12. Semilogarithmic plot of conversion of benzene as a function of TOS for hydrothermally and hydrothermally + iron-modified ZSM-5 zeolites. $W/F = 20\ \mathrm{kg_{cat}\,s/mol}$, $C_6H_6/N_2O/N_2 \approx 4/2/1$ (molar), $S > 95\%$, 425 °C (values in brackets not taken into account for regression).

Table 5
Data on catalytic performance of postsynthetically iron-modified materials[a]

	400 °C		425 °C		450 °C	
	k_d (h^{-1})	X_0 (%)	k_d (h^{-1})	X_0 (%)	k_d (h^{-1})	X_0 (%)
A-650st-1	0.23	6	0.29	7	0.39	8
A-st-1-Fe	0.31	10	0.43	11	0.61	16
A-st-1-Fe-S2O4	0.43	11	0.56	14	0.77	17
A-st-1-Fe-S2O4ac	0.30	11	0.37	13	0.55	17

[a] Reaction conditions: $W/F = 20\ \mathrm{kg_{cat}\,s/mol}$, $C_6H_6/N_2O/N_2 \approx 4/2/1$ (molar), $S > 95\%$.

4. Conclusion

For a wide variety of dealumination methods, the catalytic performance of two HZSM-5 zeolites with slightly different Fe contents for the direct hydroxylation of benzene with N_2O is described on the basis of the physicochemical properties of the resulting materials. Brønsted acidity was identified as the key factor of deactivation rate. Under the reaction conditions studied it seems realistic to obtain catalysts nearly free of activity loss, if even lower levels of Brønsted acidity could be achieved. In accordance with the ideas of Motz et al. [6] and Kustov et al. [9], catalytic activity can be described by the level of Lewis acidity created upon dealumination, when taking into account that the reaction is limited by micropore diffusion; thus the formation of mesopores is a crucial step in order to enable access to these sites. The results of the present study also corroborate the recent findings of Hensen et al. [14], who proposed Lewis acid extraframework Al–O–Fe entities as active species.

Materials with intentional addition of Fe, either during hydrothermal synthesis or in a postsynthetic modification step, hardly fit this pattern. Together with the different shapes of deactivation curves it is assumed that catalysis

and loss of activity on these materials proceed via different mechanisms.

The most favorable catalyst in the present study was obtained by solid-state isomorphous substitution of FAL by $(NH_4)_2SiF_6$ and subsequent thermal treatment. The removal of Brønsted acid sites is most efficient and simultaneously a substantial level of Lewis acidity and mesoporosity can be created.

References

[1] E. Suzuki, K. Nakashiro, Y. Ono, Chem. Lett. (1988) 953.
[2] M. Gubelmann, P.J. Tirel, US patent 5001280 (1991), to Rhone-Poulenc Chimie.
[3] R. Burch, C. Howitt, Appl. Catal. A 86 (1992) 139.
[4] G.I. Panov, A.K. Uriarte, M.A. Rodkin, V.I. Sobolev, Catal. Today 41 (1998) 365.
[5] G.I. Panov, Cattech 4 (2000) 18.
[6] J.L. Motz, H. Heinichen, W.F. Hölderich, Stud. Surf. Sci. Catal. 105 (1997) 1053.
[7] M. Häfele, A. Reitzmann, D. Roppelt, G. Emig, Appl. Catal. A 150 (1997) 153.
[8] B. Louis, L. Kiwi-Minsker, P. Reuse, A. Renken, Ind. Eng. Chem. Res. 40 (2001) 1454.
[9] L.M. Kustov, A.L. Tarasov, V.I. Bogdan, A.A. Tyrlov, J.W. Fulmer, Catal. Today 61 (2000) 123.
[10] P. Notté, Top. Catal. 13 (2000) 387.
[11] P. Kubánek, B. Wichterlová, Z. Sobalík, J. Catal. 211 (2002) 109.
[12] A. Ribera, I.W.C.E. Arends, S. de Vries, J. Perez-Ramirez, R.A. Sheldon, J. Catal. 195 (2000) 287.
[13] D. Meloni, R. Monaci, V. Solinas, G. Berlier, S. Bordiga, I. Rossetti, C. Oliva, L. Forni, J. Catal. 214 (2003) 169.
[14] E.J.M. Hensen, Q. Zhu, R.A. van Santen, J. Catal. 220 (2003) 260.
[15] A.S. Kharitanov, G.A. Sheleva, G.I. Panov, V.I. Sobolev, Y.A. Paukshits, V.N. Romannikov, Appl. Catal. A 98 (1993) 33.
[16] K.A. Dubkov, N.S. Ovanesyan, A.A. Shteinmann, E.V. Stakaron, G.I. Panov, J. Catal. 207 (2002) 341.
[17] W.D. McGhee, US patent 5808167 (1998), to Solutia Inc.
[18] A. Reitzmann, G. Emig, E. Klemm, S. Kowalak, K. Nowinska, DE patent 19829515 A1 (1998).
[19] J. Jia, K.S. Pillai, W.M.H. Sachtler, J. Catal. 221 (2004) 119.
[20] Q. Zhu, R.M. van Teeffelen, R.A. van Santen, E.J.M. Hensen, J. Catal. 221 (2004) 575.
[21] J.L. Motz, W.F. Hölderich, H. Heinichen, DE patent 19634406 (1998), to Hoechst AG.
[22] F. Kollmer, H. Hausmann, W.F. Hölderich, J. Catal., accepted.
[23] A.K. Uriarte, M.A. Rodkin, M.J. Gross, A.S. Kharitanov, G.I. Panov, Stud. Surf. Sci. Catal. 110 (1997) 857.
[24] W.D. McGhee, P.P.B. Notté, US patent 5874647 (1999), to Solutia Inc.
[25] R. Burch, C. Howitt, Appl. Catal. A 106 (1993) 167.
[26] D.P. Ivanov, M.A. Rodkin, K.A. Dubkov, A.S. Kharitanov, G.I. Panov, Kinet. Catal. 41 (2000) 850.
[27] W.F. Hoelderich, F. Kollmer, Pure Appl. Chem. 72 (2000) 1273.
[28] W.F. Hoelderich, F. Kollmer, Catalysis 16 (2002) 43.
[29] L.M. Kustov, V.I. Bogdan, V.B. Kazansky, EP patent 0889018 A1 (1998), to General Electric Company, Zelinsky Institute of Organic Chemistry.
[30] M. Baerns, H. Hofmann, A. Renken, Chemische Reaktionstechnik, Thieme, Stuttgart, 1992.
[31] J. Kärger, D.M. Ruthven, Diffusion in Zeolites, Wiley, New York, 1992.
[32] H.-J. Doelle, J. Heering, L. Riekert, L. Marosi, J. Catal. 71 (1981) 27.
[33] L.V. Pirutko, V.S. Chernyavsky, A.K. Uriarte, G.I. Panov, Appl. Catal. A 227 (2002) 143.
[34] G. Kuehl, in: J. Weitkamp, L. Puppe (Eds.), Catalysis and Zeolites—Fundamentals and Applications, Springer, Berlin, 1999, p. 81.
[35] E. Derouane, M. Mestdagh, L. Vielvoye, J. Catal. 33 (1974) 169.
[36] H. Karge, M. Hunger, H.K. Beyer, in: J. Weitkamp, L. Puppe (Eds.), Catalysis and Zeolites—Fundamentals and Applications, Springer, Berlin, 1999, p. 198.
[37] E. Loeffler, C. Peuker, H.G. Jerschkewitz, Catal. Today 3 (1988) 415.
[38] M. Müller, G. Harvey, R. Prins, Micropor. Mesopor. Mater. 34 (2000) 135.
[39] M. Müller, G. Harvey, R. Prins, Micropor. Mesopor. Mater. 34 (2000) 281.
[40] M.C. Cruickshank, L.S. Dentglesser, S.A.I. Barri, J. Chem. Soc., Chem. Commun. (1986) 23.
[41] W.A. Buckermann, C.B. Huong, F. Fajula, Zeolites 13 (1993) 410.
[42] J.P. Gilson, G.C. Edwards, A.W. Peters, K. Rajagopalan, R.F. Wormsbecher, T.G. Roberie, M.P. Shatlock, J. Chem. Soc., Chem. Commun. (1987) 91.
[43] J. Sanz, V. Fornés, A. Corma, J. Chem. Soc., Faraday Trans. 84 (1988) 3113.
[44] E. Brunner, H. Ernst, D. Freude, M. Hunger, C.B. Krause, D. Prager, W. Reschetilowski, W. Schwieger, K.H. Bergk, Zeolites 9 (1989) 282.
[45] D. Freude, M. Hunger, H. Pfeifer, Z. Phys. Chem., NF 152 (1987) 171.
[46] A. Samoson, E. Lipmaa, G. Engelhardt, U. Lohse, H.G. Jerschkewitz, Chem. Phys. Lett. 134 (1987) 589.
[47] V.B. Kazansky, Catal. Today 3 (1988) 367.
[48] I. Kiricsi, C. Flego, G. Pazzuconi, W.O. Parker Jr., R. Millini, C. Perego, G. Bellussi, J. Phys. Chem. 98 (1994) 4627.
[49] R.M. Lago, W.O. Haag, R.J. Minkovsky, D.H. Olson, S.H. Hellring, K.P. Schmidt, G.T. Kerr, Stud. Surf. Sci. Catal. 28 (1986) 677.
[50] E. Loeffler, U. Lohse, C. Peuker, G. Oehlmann, L.M. Kustov, V.L. Zholobenko, V.B. Kazansky, Zeolites 10 (1990) 266.
[51] C. Jia, P. Massiani, D. Barthomeuf, J. Chem. Soc., Faraday Trans. 89 (1993) 3659.
[52] M. Hunger, S. Ernst, S. Steuernagel, J. Weitkamp, Micropor. Mater. 6 (1996) 349.
[53] V.M. Mastikhin, I.L. Mudrakovsky, A. Nosov, Prog. NMR Spectrosc. 23 (1991) 259.
[54] A.G. Ashton, S. Batmanian, J. Dwyer, I.S. Elliot, F.R. Fitch, J. Mol. Catal. 34 (1986) 73.
[55] S.M. Campbell, D.M. Bibby, J.M. Coddington, R.F. Howe, R.H. Meinhold, J. Catal. 161 (1996) 338.
[56] D. Coster, A.L. Blumenfeld, J.J. Fripiat, J. Phys. Chem. 98 (1994) 6201.
[57] J. Dwyer, F.R. Fitch, G. Qin, J.V. Vickermann, J. Phys. Chem. 86 (1982) 4574.
[58] L.D. Fernandes, P.B. Bartl, J.L.F. Monteiro, J.G. da Silva, S.G. de Menezes, M.J.B. Cardoso, Zeolites 14 (1994) 533.
[59] C.A. Emeis, J. Catal. 141 (1993) 347.
[60] J. Datka, A.M. Tutek, J.H. Jehng, I.E. Wachs, J. Catal. 135 (1992) 186.
[61] T.R. Hughes, H.M. White, J. Phys. Chem. 71 (1967) 2192.
[62] K.H. Rhee, U.S. Rao, J.M. Stencel, G.A. Melson, J.E. Crawford, Zeolites 3 (1983) 337.
[63] A.A. Slinkin, A.L. Klyachko, M.S. Kharson, V.D. Nissenbaum, G.O. Bragina, A.V. Kucherov, L.I. Karagulyan, I.L. Aleksandrova, Kinet. Catal. 34 (1993) 369.
[64] E. Brunner, H. Ernst, D. Freude, T. Fröhlich, M. Hunger, H. Pfeifer, J. Catal. 127 (1991) 34.
[65] A. Kohara, N. Katada, M. Niwa, Stud. Surf. Sci. Catal. 135 (2001) 2030.
[66] C. Mirodatos, D. Barthomeuf, J. Chem. Soc., Chem. Commun. (1981) 39.
[67] R.B. Borade, A. Clearfield, Micropor. Mater. 2 (1994) 167.
[68] J. Datka, T. Abramowicz, J. Chem. Soc., Faraday Trans. 90 (1994) 2417.
[69] J.A. Martens, W. Souverijns, W. van Rhijn, P.A. Jacobs, in: G. Ertl, H. Knözinger, J. Weitkamp (Eds.), Handbook of Heterogeneous Catalysis, vol. 1, VCH–Wiley, Weinheim, 1997, p. 325.

[70] J. Pérez-Ramírez, G. Mul, F. Kapteijn, J.A. Mouljin, A.R. Overweg, A. Doménech, A. Ribera, I.W.C.E. Arends, J. Catal. 207 (2002) 113.
[71] B. Vogel, C. Schneider, E. Klemm, Catal. Lett. 79 (2002) 107.
[72] O. Levenspiel, Chemical Reaction Engineering, Wiley, New York, 2000.
[73] P.B. Weisz, Z. Phys. Chem. 11 (1957) 1.
[74] J. Völter, G. Lietz, U. Kürschner, E. Löffler, J. Caro, Catal. Today 3 (1988) 407.
[75] G.L. Woolery, G.H. Kuehl, H.C. Timken, A.W. Chester, J.C. Vartuli, Zeolites 19 (1997) 288.
[76] R.D. Shannon, C.T. Prewitt, Acta Crystallogr. B 25 (1969) 925.
[77] E. Klemm, J. Wang, G. Emig, Micropor. Mesopor. Mater. 26 (1998) 11.
[78] N.Y. Chen, P.B. Weisz, Chem. Eng. Prog., Symp. Ser. 63 (1967) 86.
[79] V.S. Nayak, L. Rieckert, Acta Phys. Chem. 31 (1985) 157.
[80] N.-Y. Topsoe, K. Pedersen, E. Derouane, J. Catal. 70 (1981) 41.